https://doi.org/10.5194/acp-2020-978
Preprint. Discussion started: 29 October 2020

Atmospheric Chemistry and Physics Discussions

Role of oceanic ozone deposition in explaining short-term variability of Arctic surface ozone

Johannes G.M. Barten[1], Laurens N. Ganzeveld[1], Gert-Jan Steeneveld[1], and Maarten C. Krol[1,2]

[1]Wageningen University, Meteorology and Air Quality Section, Wageningen, the Netherlands
[2]Institute for Marine and Atmospheric Research Utrecht, Utrecht University, Utrecht, the Netherlands

Correspondence: Johannes G.M. Barten (sjoerd.barten@wur.nl)

Abstract. Dry deposition is an important removal mechanism for tropospheric ozone (O_3). Currently, O_3 deposition to oceans in atmospheric chemistry and transport models (ACTMs) is generally represented using constant surface uptake resistances. This is despite the fact that considering the role of solubility, waterside turbulence and O_3 reacting with ocean water reactants such as iodide and dissolved organic matter results in substantial spatiotemporal variability in O_3 deposition and concentrations in marine boundary layers. We hypothesize that O_3 deposition to the cold Arctic ocean, with relatively low reactivity, is also overestimated in current models with consequences for background concentrations, lifetime of O_3 and long-range transport of O_3. In this study, we investigate the role of the representation of oceanic O_3 deposition to the simulated magnitude and spatiotemporal variability in Arctic surface O_3. This study also serves as a preparatory study to understand the year-round Arctic O_3 concentration and deposition flux measurements as part of the MOSAiC field campaign. Furthermore, it is also important to enhance our understanding and quantification of Arctic ocean-atmosphere exchange of O_3 and other climate-active trace gases given the anticipated opening of the Arctic ocean.

We have coupled the Coupled Ocean-Atmosphere Response Experiment Gas transfer algorithm (COAREG) to the mesoscale meteorology and atmospheric chemistry model Polar-WRF-Chem (WRF) and introduced a dependence of O_3 deposition on ocean waterside turbulent mixing conditions and biogeochemical composition. We have also reduced the O_3 deposition to sea ice and snow. Here, we evaluate the performance of WRF and the CAMS reanalysis data against hourly-averaged surface O_3 observations at 25 sites (latitudes > 60 ºN) including the ASCOS campaign observations. This is the first time such a coupled modelling system has been evaluated against hourly observations at Pan-Arctic sites to study the sensitivity of the deposition scheme to the magnitude and short-term temporal variability in Arctic surface O_3. We also analyze the impact of nudging WRF to the synoptic conditions from the ECMWF ERA5 reanalysis data on simulated Arctic meteorology and comparison of observed and simulated O_3 concentrations.

We show that the more mechanistic representation of O_3 deposition over oceans and reduced snow/ice deposition improves simulated Arctic O_3 mixing ratios both in terms of magnitude but also regarding observed temporal variability. Using the newly implemented approach, O_3 deposition velocities have been simulated in the order of 0.01 cm s^{-1} compared to ~0.05 cm s^{-1} in the constant surface uptake resistance approach. The simulated spatial variability in the mechanistic approach (0.01 to 0.018 cm s^{-1}) expresses the sensitivity to chemical enhancement with dissolved iodide whereas the temporal variability (up to ± 20% around the mean) expresses differences in waterside turbulent transport. The bias for all observational sites

https://doi.org/10.5194/acp-2020-978
Preprint. Discussion started: 29 October 2020


Atmospheric Chemistry and Physics Discussions

above 70 ºN reduced from -7.7 ppb to 0.3 ppb with nudging and the revision to ocean and snow/ice deposition. Our study confirms that O_3 deposition to oceans and snow/ice is overestimated in current models. We recommend that a mechanistic representation of oceanic O_3 deposition is used in ACTMs to improve the representation of Arctic surface O_3 concentrations in terms of magnitude and short-term temporal variability. The revised ocean-atmosphere exchange representation can be further refined using the MOSAiC flux measurements as well as complementary observations such as sea ice and ocean water iodide concentrations.

1 Introduction

Tropospheric Ozone (O_3) is the third most important greenhouse gas and a secondary air pollutant negatively affecting human health (Nuvolone et al., 2018) and plant growth (Ainsworth et al., 2012) due to its oxidative character. O_3 shows a large spatiotemporal variability due to its relatively short lifetime (3-4 weeks) compared to other greenhouse gases. Its main sources are chemical production and entrainment from the stratosphere. Its main sinks are chemical destruction and deposition to the Earth's surface. Understanding the Arctic O_3 budget is of particular interest because its remote location implies that anthropogenic sources and sinks are generally absent. This makes these background O_3 observations an excellent indicator for global trends (Helmig et al., 2007b; Gaudel et al., 2020). In the Arctic, routine tropospheric O_3 observations indicate an increasing trend up to the early 2000s which is leveling off in the last decade (Oltmans et al., 2013; Cooper et al., 2014). This upward trend can be attributed to increased emissions of precursors in the mid-latitudes (Cooper et al., 2014) but also stratosphere-to-troposphere transport may have played a role (Pausata et al., 2012). Local emissions of precursors are expected to become an important source of Arctic O_3 concentrations due to the warming Arctic climate and increasing local economic activity (Marelle et al., 2016; Law et al., 2017). This stresses the need to better understand the sources and sinks of Arctic tropospheric O_3 and to accurately represent them in atmospheric chemistry and transport models (ACTMs).

On the global scale, dry deposition accounts for ∼25% of the total sink term (Lelieveld and Dentener, 2000) in ACTM simulations and is especially important for the O_3 budget in the Atmospheric Boundary Layer (ABL) because it occurs at the Earth's surface (Hardacre et al., 2015). Dry deposition in such model assessments is often represented as a resistance in series approach (Wesely, 1989). In this approach the total resistance r_t is the sum of three serial resistances: the aerodynamic resistance (r_a) representing turbulent transport to the surface, the quasi-laminar sub layer resistance (r_b) representing diffusion close to the surface and the surface resistance (r_s) expressing the efficiency of removal by the surface. The dry deposition velocity (V_d) is then evaluated as the reciprocal of r_t. For very soluble species or reactive species such as nitric acid uptake by the ocean water is very fast, expressed by a r_s of ∼0 s m^{-1}, implying that the other resistances determine r_t and thus V_d. Less soluble gases, like O_3, have a high r_s that mainly dominates the magnitude of the O_3 dry deposition velocity (V_{d,O_3}). Thus, accurately representing the surface uptake efficiency is of high importance.

Even though O_3 deposition to oceans is relatively slow compared to terrestrial surfaces, expressed by typically observed ocean V_{d,O_3} of ∼0.01-0.1 cm s^{-1} (e.g. Helmig et al., 2012) compared to observed maximum V_{d,O_3} for forests up to 2 cm s^{-1}, it plays a large role in the total deposition budget due to the large surface area of water bodies (Ganzeveld et al., 2009). Recent exper-

https://doi.org/10.5194/acp-2020-978
Preprint. Discussion started: 29 October 2020


Atmospheric Chemistry and Physics Discussions

imental and modelling studies indicate the spatiotemporal variability in oceanic O_3 uptake efficiency (Ganzeveld et al., 2009; Helmig et al., 2012; Luhar et al., 2018). However, most models often still use a constant O_3 surface uptake efficiency to water bodies resulting in a simulated ocean V_{d,O_3} of ~0.05 cm s^{-1}. The observed V_{d,O_3} shows a larger variability including also a dependency on wind speed and Sea Surface Temperature (SST) (Helmig et al., 2012). The dependency on wind speed also expresses an enhancement of O_3 deposition due to waterside turbulence (Fairall et al., 2007). This turbulence driven enhancement is complemented by a strong chemical enhancement of oceanic O_3 deposition associated with its chemical destruction through oxidation of ocean water reactants such as dissolved iodide and dissolved organic matter (DOM) (Chang et al., 2004). Mechanistic O_3 deposition representations include the physical and biogeochemical processes related to the exchange and destruction of O_3 in surface waters (Fairall et al., 2007, 2011; Ganzeveld et al., 2009; Luhar et al., 2017, 2018). Dissolved iodide is deemed to be the main reactant of O_3 in surface waters (Chang et al., 2004) and therefore often applied in these representations. Some studies only consider dissolved iodide as a reactant (Luhar et al., 2017; Pound et al., 2019) whereas Ganzeveld et al. (2009) also included DOM as one reactant contributing to the chemical enhancement of oceanic O_3 deposition. However, the role of DOM in oceanic O_3 deposition remains difficult to quantify and which appears to be mainly addressed by controlled laboratory measurements or O_3 flux measurements at sites with elevated DOM water concentrations.

Nevertheless, application of these more mechanistic ocean O_3 deposition representations illustrated the importance of a more explicit representation of O_3 dry deposition in ACTMs, not only regarding the impact on marine ABL O_3 concentrations and budget, but also to consider potentially important feedback mechanisms. For instance, the implementation of these mechanistic exchange methods in ACTMs indicates a ~50% reduction of the global mean V_{d,O_3} which affects the tropospheric O_3 burden (Pound et al., 2019). This mechanistic representation especially results in a simulated decrease in V_{d,O_3} to cold polar waters with relatively low reactivity. Simulated V_{d,O_3} can be as low as 0.01 cm s^{-1} compared to the commonly applied V_{d,O_3} of 0.05 cm s^{-1} in the constant surface uptake resistance approach (Pound et al., 2019). Regarding feedback mechanisms, consideration of the mechanisms that ultimately determine the efficiency of uptake and destruction of O_3 in ocean surface waters might also explain the release of halogen compounds into the ABL (Prados Roman et al., 2015). These halogen compounds, in turn, are involved in O_3 depletion in the ABL and therefore reduce further uptake and destruction of O_3 in ocean surface waters implying existence of a negative feedback mechanism.

Up until now, earlier studies have mostly focused on the effects on the global scale (Ganzeveld et al., 2009; Luhar et al., 2017) using monthly mean surface O_3 observations (Pound et al., 2019). However, the hypothesized reduction in O_3 deposition to cold waters is also expected to substantially affect Arctic ABL O_3 concentrations on shorter timescales and potentially improve operational Arctic O_3 forecasts, e.g. the air quality forecasts by the Copernicus Atmosphere Monitoring Service (CAMS) (Inness et al., 2019). An improved representation of sub-monthly Arctic O_3 concentrations helps to constrain the background O_3 concentrations in terms of magnitude and variability whereas the evaluation of simulated oceanic O_3 deposition in the Arctic is hampered by a lack of O_3 ocean-atmosphere flux observations. Hence, evaluation of simulated O_3 deposition relies on evaluation of surface O_3 concentrations, in particular on the highly resolved temporal variability. We hypothesize that on the daily and diurnal timescales these concentrations largely controlled by temporal variability in the main physical drivers of oceanic O_3 deposition, e.g. atmospheric and waterside turbulence. Chemical enhancement of, e.g., iodide to O_3 deposition is anticipated

https://doi.org/10.5194/acp-2020-978
Preprint. Discussion started: 29 October 2020


Atmospheric Chemistry and Physics Discussions

to control more the long-term (weeks-months) baseline level of V_{d,O_3} associated with anticipated more long-term changes in ocean water biogeochemical conditions. This evaluation of Arctic O_3 concentrations in terms of magnitude and short- and long-term variability aims to better understand sinks, processes, feedbacks and impacts of Arctic air pollution (Arnold et al., 2016) and the role of long-range transport (e.g. Thomas et al., 2013; Marelle et al., 2018) versus local sources (e.g. Marelle et al., 2016; Law et al., 2017; Schmale et al., 2018). Furthermore, the anticipated opening of the Arctic ocean, as one of the key features of Arctic climate change, urges to improve our understanding of Arctic ocean-atmosphere exchange. In this study we only focus on the ocean-atmosphere exchange of O_3, but follow-up studies are planned with a focus on ocean-atmosphere exchange and ABL concentrations of other trace gases such as dimethylsulfide (DMS), which enhances cloud formation and is involved in many feedback mechanisms (Mahmood et al., 2019).

The main objective of this study is to address the role of a mechanistic representation of O_3 deposition in explaining observed hourly Arctic surface O_3 concentrations, both in terms of magnitude and temporal variability. A coupled meteorology-atmospheric chemistry model is set up for an end-of-summer period in 2008 and evaluated against a large dataset of pan-Arctic O_3 observations at a high resolution (hourly) timescale. Having a much higher spatial and temporal resolutions compared to other global modelling studies we aim to better capture the role of spatiotemporal variability in O_3 deposition in explaining observed surface O_3 concentrations in particular regarding temporal variability. We also indicate the role of meteorology in simulating these O_3 concentrations by nudging the simulated synoptic conditions towards an atmospheric reanalysis dataset. This study also serves as a preparatory study to understand the year-round Arctic O_3 concentration and deposition flux measurements including the role of the local meteorology such as boundary layer mixing and entrainment as part of the Multidisciplinary drifting Observatory for the Study of Arctic Climate (MOSAiC) campaign (mosaic-expedition.org, last access: 16 September 2020). Section 2 describes the adjustments to the deposition scheme, further model setup and observational datasets. Section 3 presents the main results of the study which are further discussed in Sect. 4. This manuscript is finalized with the conclusions in Sect. 5.

2 Methods

2.1 Regional coupled meteorology-chemistry model

We use the Weather Research and Forecasting model (v4.1.1) coupled to chemistry (Chem) (Grell et al., 2005) and optimized for Polar regions (Hines and Bromwich, 2008). Polar-WRF-Chem (hereafter: WRF) is a non-hydrostatic mesoscale numerical weather prediction and atmospheric chemistry model used for operational and research purposes. Figure 1 shows the selected study area including the locations of surface O_3 observational sites that will be used in this study. WRF is set up with a polar projection centered at 90°N, 250×250 horizontal grid points (30×30 km resolution) and 44 vertical levels up to 100 hPa, with a finer vertical grid spacing in the ABL and lower troposphere. The simulation period is 08-08-2008 to 07-09-2008 including three days of spin-up. This end-of-summer 2008 period is chosen for two reasons: 1) to limit the role of halogen chemistry during springtime (Pratt et al., 2013; Thompson et al., 2017) and 2) the additional availability of O_3 observations in the high Arctic over sea ice from the ASCOS campaign (Paatero et al., 2009). The ECMWF ERA5 meteorology (0.25°×0.25°)

https://doi.org/10.5194/acp-2020-978
Preprint. Discussion started: 29 October 2020

Atmospheric Chemistry and Physics Discussions

(Hersbach et al., 2020) and CAMS reanalysis chemistry (0.75°×0.75°) (Inness et al., 2019) products are used for the initial and boundary conditions. Boundary conditions, SSTs and sea ice fractions are updated every three hours to these reanalysis
130 products to allow for the sea ice retreat during the simulation. Other relevant parameterization schemes and emission datasets have been listed in Tab. A1 and are mostly based on Bromwich et al. (2013).

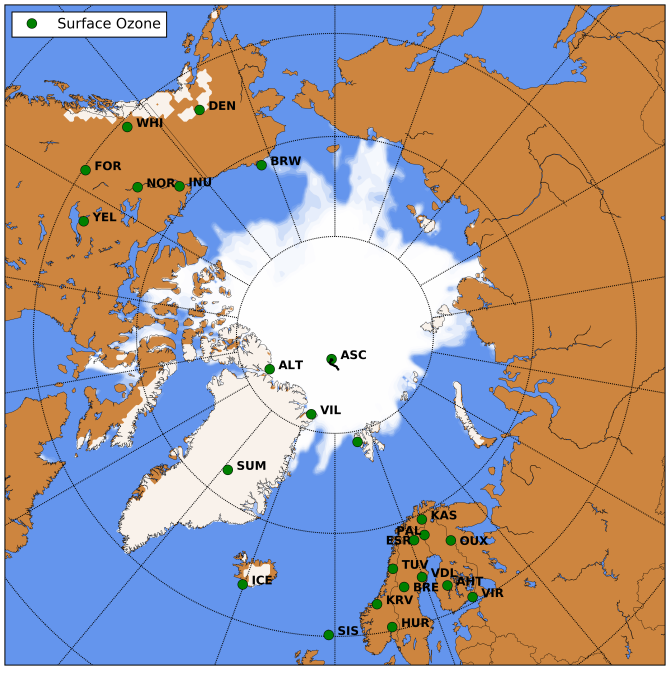

Figure 1. WRF domain including sea ice and snow cover at the start of the simulation. Locations with surface observations O_3 are indicated in green. The drifting path of the ASCOS campaign during the simulation is indicated with the black line.

2.1.1 Nudging to ECMWF ERA5

The first WRF simulation, without any adjustments to O_3 deposition, indicated that WRF was misrepresenting the temporal variability in surface O_3 observations, most prominently starting from a few days into the simulation. We hypothesize that
135 these deviations are caused by deviations in the synoptic conditions in the free running WRF simulation. To verify this, WRF results are compared against the observations from the Advanced Microwave Scanning Radiometer - Earth Observing System (AMSR-E) sensor on NASA's Aqua satellite. The near surface wind speeds above oceans from the Daily Level-3 data product are used with a spatial resolution of 0.25°×0.25° (Wentz and Meissner, 2004).

Figure 2 shows the temporal evolution in the bias (WRF minus AMSR-E) and Mean Absolute Error (MAE) of the daily and
140 ocean grid box averaged 10-m wind speeds. The first days there is no clear bias. However, later in the simulation we find a persistent bias indicating that WRF overestimates the wind speeds above the Arctic ocean. During the first days the MAE amounts to ∼1.5 m s^{-1}, while later in the simulation the MAE reaches 2.5-3.0 m s^{-1}. To overcome the impact of this deficiency

https://doi.org/10.5194/acp-2020-978
Preprint. Discussion started: 29 October 2020

Atmospheric Chemistry and Physics Discussions

on our O_3 budget study, nudging is applied to ensure a fair model evaluation with observations. Hence, WRF is nudged every three hours to the ECMWF ERA5 humidity, temperature and wind fields in the free troposphere with nudging coefficients of $1 \cdot 10^{-5}$ s^{-1}, $3 \cdot 10^{-4}$ s^{-1} and $3 \cdot 10^{-4}$ s^{-1}, respectively. In Sect. 3.3 the role of nudging on simulated surface O_3 is further analysed.

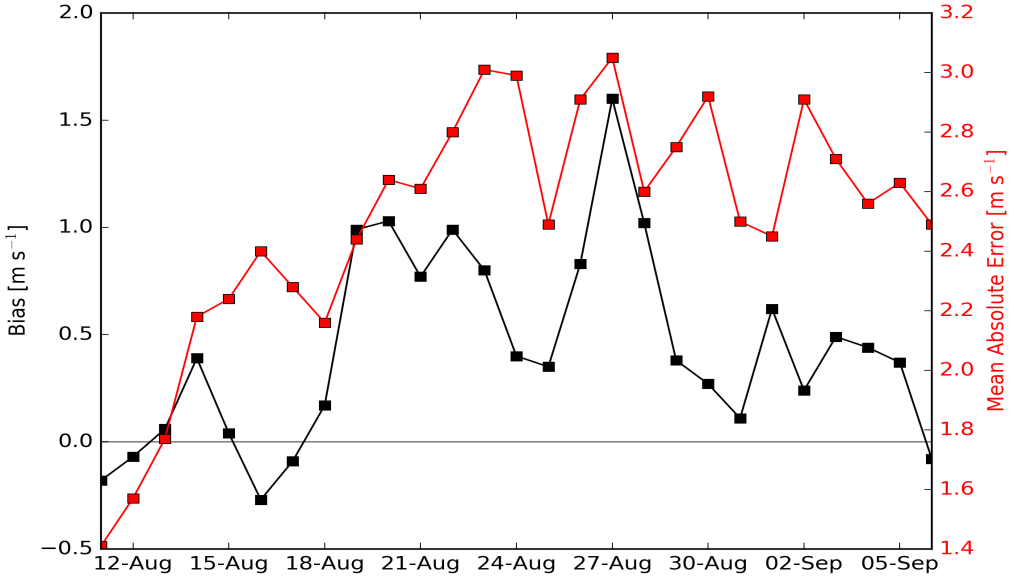

Figure 2. Temporal evolution of the bias (WRF minus AMSR-E, black) [m s^{-1}] and Mean Absolute Error (MAE, red) [m s^{-1}] of 10-m wind speeds above oceans for the period of 11-Aug to 6-Sep 2008. Note that the right y-axis starts at 1.4 m s^{-1}.

145

2.2 Representation of ocean-atmosphere gas exchange

The Coupled Ocean-Atmosphere Response Experiment (COARE) (Fairall et al., 1996) has been developed to study physical exchange processes (sensible heat, latent heat and momentum) at the ocean-atmosphere interface. Later, COARE has been extended to include the exchange of gaseous species such as O_3, dimethyl sulfide (DMS) and carbon dioxide (CO_2) (Fairall
150 et al., 2011). Many studies have used the COARE Gas transfer algorithm (COAREG) in combination with eddy covariance measurements to study the effects of wind speed and sea state on ocean-atmosphere gas exchange (e.g. Helmig et al. (2012), Blomquist et al. (2017), Bell et al. (2017), Porter et al. (2020)). Furthermore, the COAREG algorithm has also been previously used in global O_3 modelling studies Ganzeveld et al. (2009). The choice for COAREG as ocean-atmosphere exchange parameterization is further motivated by the consistent coupling with other species such as DMS.

155 Here we use COAREG version 3.6, which is extended with a two-layer scheme for surface resistance compared to the previous version described by Fairall et al. (2007, 2011). COAREG version 3.6 has already been used in a study by Porter et al. (2020) on air-sea transfer of highly soluble species. The two-layer scheme is similar to the work by Luhar et al. (2018) building upon

https://doi.org/10.5194/acp-2020-978
Preprint. Discussion started: 29 October 2020


Atmospheric Chemistry and Physics Discussions

a first application of a 1-layer version of COAREG for oceanic O_3 deposition in a global modelling study by Ganzeveld et al. (2009). In that study, chemical enhancement of ocean O_3 deposition by its reaction with iodide was considered using a global climatology of ocean surface water concentrations of nitrate serving as a proxy for oceanic iodide concentrations (I^-_{aq}), the compound that is generally deemed to be the most significant reactant for O_3 in ocean water (Chang et al., 2004). Since then, alternative parameterizations of oceanic I^-_{aq} have been proposed (e.g. MacDonald et al., 2014) using SST as a proxy for this reactant. In COAREG, chemical reactivity of O_3 with I^-_{aq} is present through the depth of the oceanic mixing layer. O_3 loss by waterside turbulent transfer is negligible in the top water layer (few micrometers), but is accounted for in the underlying water column. The waterside turbulent transfer term is especially relevant for relatively cold waters because the chemical enhancement term is then relatively low (Fairall et al., 2007; Ganzeveld et al., 2009; Luhar et al., 2017). The last two important waterside processes that determine the total O_3 deposition are molecular diffusion and solubility of O_3 in seawater which both depend on the SST.

In this study, the COAREG algorithm is coupled such that WRF provides the meteorological and SST input for the COAREG routine. In turn, the COAREG calculated ocean-atmosphere exchange velocities are used in the WRF model to calculate the total flux. This study focuses on the exchange, in this case deposition, of O_3. The oceanic O_3 deposition fluxes replace the default deposition fluxes calculated by the Wesely (1989) scheme. For grid boxes with fractional sea ice cover, COAREG replaces the Wesely deposition scheme for the fraction that is ice free.

Moreover, we apply the I^-_{aq} distribution by Sherwen et al. (2019) ($0.125° \times 0.125°$ resolution). This distribution does not only depend on SST, but applies a machine learning approach using various physical and chemical variables. For high latitudes, this implies higher I^-_{aq} and thus higher O_3 deposition compared to MacDonald et al. (2014). In that study, I^-_{aq} is solely a function of SST which leads to very small I^-_{aq} in the cold Arctic ocean and thus low reactivity and O_3 deposition velocities.

As mentioned previously, the study by Ganzeveld et al. (2009) also considered the potentially important enhancement in oceanic O_3 deposition by its reaction with DOM, a feature not considered in studies by Luhar et al. (2017); Pound et al. (2019). In Sect. 4 we will discuss the potential role of DOM in our simulations and Arctic O_3 deposition.

2.2.1 Deposition to snow and ice

Reported atmosphere-snow gas exchange spans a wide range of observed O_3 deposition velocities. Some studies even report episodes of negative deposition fluxes (emissions) over snow or sea ice (Zeller, 2000; Helmig et al., 2009; Muller et al., 2012). Helmig et al. (2007a) investigated the sensitivity of a chemistry and tracer transport model to the prescribed O_3 deposition velocity and found best agreement between modelled and observed O_3 concentrations by applying deposition velocities in the order of 0.00-0.01 cm s^{-1}. Based on Helmig et al. (2007a) we have increased the O_3 surface uptake resistance (r_s) for snow and ice land use classes to 10^4 s m^{-1}. This corresponds to total deposition velocities of $\leq$0.01 cm s^{-1}, which is a reduction of $\sim$66% compared to the Wesely deposition routine that is the default being applied in WRF. Effects of this modification are further examined in Sect. 3.1.

https://doi.org/10.5194/acp-2020-978
Preprint. Discussion started: 29 October 2020


Atmospheric Chemistry and Physics Discussions

2.3 Observational data of surface ozone

The new modelling setup, including nudging to ECMWF ERA5 and the revised O_3 deposition to snow, ice and oceans, is evaluated against observational data of pan-Arctic surface O_3. We expect that the different representation of O_3 deposition mostly affects O_3 concentrations in the ABL. Therefore, we evaluate our simulations against hourly averaged surface O_3 observations from 25 measurement sites above 60 °N. These sites are further categorized in three site selections: 'High Arctic', 'Terrestrial' and 'Remote'. High Arctic refers to sites having latitudes > 70 °N and for which we expect that the deposition footprint is a combination of ocean and (sea-)ice. The Terrestrial sites are located below 70 °N and show a clear diurnal cycle in observed O_3. These diurnal cycles are governed by a combination of emissions of precursors, but also the anticipated larger diurnal cycle in O_3 deposition to, e.g., vegetated surfaces and a stronger diurnal cycle in turbulent mixing conditions and ABL dynamics. These are in all aspects different from sites that have an ocean/ice footprint where we expect low emissions of precursors, no clear diurnal cycle in O_3 deposition and a weaker diurnal cycle in ABL dynamics. In this study, the criterion is that the average observed minimum nighttime mixing ratio is > 8 ppb smaller than the average observed maximum daytime mixing ratio during the ∼1 month of simulation. This criterion is based on a preparatory analysis of the observational data, footprint and site characteristics. The Remote sites are located below 70 °N and at which no clear diurnal cycle is observed. The analysis also includes the observations during the Arctic Summer Cloud Ocean Study (ASCOS) campaign, when the icebreaker Oden was located in the Arctic sea ice (Tjernstrom et al., 2012). In total, 25 surface O_3 measurement sites are included (Fig. 1) of which 6, 8 and 11 sites are characterized High Arctic, Remote and Terrestrial sites, respectively. A full list of available measurement sites is available in Tab. B1.

2.4 Overview of performed simulations

In total, we perform three simulations. The first WRF simulation (DEFAULT) is a run without any adjustments to the code as described in Sect. 2.1. The second simulation (NUDGED) includes nudging of the synoptic conditions to the ECMWF ERA5 product as described in Sect. 2.1.1. The third simulation (COAREG) includes nudging, but also includes the adjustments to the O_3 deposition to oceans as described in Sect. 2.2 and the O_3 deposition to snow and ice as described in Sect. 2.2.1. Furthermore, we also compare our results with the the state-of-the-art CAMS global reanalysis data product (Inness et al., 2019). This product has a temporal resolution of 3 hours, a spatial resolution of $0.75° \times 0.75°$, and does not include a mechanistic representation of ocean-atmosphere O_3 exchange. Regarding O_3, CAMS assimilates satellite observations but it does not assimilate O_3 observations from in situ measurement sites or radiosondes. Moreover, CAMS is being widely used for air quality forecasts and assessments but also to constrain regional scale modelling experiments such as presented in this study.

3 Results

First, we will present the spatial and temporal variation in O_3 dry deposition velocities (V_{d,O_3}) of the new and default modelling setup including the effect on the total O_3 deposition budget. Subsequently we will discuss the resulting effect on the spatial

https://doi.org/10.5194/acp-2020-978
Preprint. Discussion started: 29 October 2020


Atmospheric Chemistry and Physics Discussions

distribution of the mean background surface O_3 mixing ratios. Then, we will present the comparison of all WRF simulations and CAMS data with the hourly surface observations for the three site selections (High Arctic, Remote and Terrestrial). This section is finalized by the simulated and observed time series for the six High Arctic sites.

3.1 Dry deposition budgets and distribution

Figure 3a and Fig. 3b show the mean deposition velocities for the DEFAULT and COAREG runs, respectively. As expected, in the DEFAULT run (Fig. 3a) the mean V_{d,O_3} to oceans are in the order of 0.05 cm s^{-1}. Furthermore, the spatial distribution shows a relatively low heterogeneity and no increase in deposition towards the warmer waters. In the COAREG run (Fig. 3b) we find mean V_{d,O_3} in the order of 0.01 cm s^{-1} for the colder waters up to 0.018 cm s^{-1} for the warmer waters. There also appears to be an enhancement of O_3 deposition to coastal waters (e.g. Baltic Sea and around the Bering Strait) with I^-_{aq} concentrations reaching up to 130 nM compared to 30 nM for the open Arctic ocean waters (not shown here). This highlights the sensitivity of the COAREG scheme to chemical enhancement with dissolved iodide. Figure 3c shows the temporal variability in V_{d,O_3} for one of the grid boxes, which is in terms of temporal variability representative for the whole domain. The temporal variability in the DEFAULT run is governed by temporal variability in r_a. During episodes with high wind speeds (> 10 m s^{-1}), r_a becomes so small that it is negligible over the constant surface uptake resistance of 2000 s m^{-1}, corresponding to a maximum V_{d,O_3} of 0.05 cm s^{-1}. During episodes with low wind speeds (< 5 m s^{-1}), reduced turbulent transport poses some additional restriction on O_3 removal with increasing r_a which can reduce the V_{d,O_3} up to $\sim$8%. In the COAREG run, the temporal variability in O_3 deposition is also governed by wind speeds that controls the waterside turbulent transport of O_3 in seawater besides atmospheric turbulent transport. For high wind speeds, the waterside turbulent transport increases and more O_3 is transported through the turbulent layers. For our simulation, we found that the temporal variability in O_3 deposition due to waterside turbulent transport can be up to $\pm$20% around the mean. Overall, the V_{d,O_3} to oceans in the COAREG run is reduced by $\sim$60-80% compared to the DEFAULT run. The mean V_{d,O_3} to snow and ice is reduced by $\sim$30%, from $\sim$0.03 cm s^{-1} in the DEFAULT run to $\sim$0.01 cm s^{-1} in the COAREG run.

By estimating the total deposition flux for the water, snow/ice and land surfaces we can quantify the total simulated O_3 deposition budget (Tab. 1) for the Arctic modelling domain. Land, not covered with snow or ice, is with 48% the dominant surface type for this specific domain setup in summer. Combined with a relatively high simulated V_{d,O_3} of $\sim$0.45 cm s^{-1} this is the most important sink, in terms of deposition, of simulated O_3 with $\sim$136 Tg O_3 yr^{-1}. The simulated O_3 deposition budget to water bodies, covering 37% of the total surface area, is in the DEFAULT run $\sim$10% ($\sim$15.5 Tg O_3 yr^{-1}) of the total O_3 deposition sink. In the COAREG run, this reduces to only $\sim$3% ($\sim$4.6 Tg O_3 yr^{-1}) of the total O_3 deposition sink. Simulated O_3 deposition to snow and ice, covering 15% of the total surface area, is the least important deposition sink with $\sim$4.1 and $\sim$1.7 Tg O_3 yr^{-1} for the DEFAULT and COAREG runs respectively.

3.2 Simulated and observed monthly mean surface ozone

The reduction in O_3 deposition to water and snow/ice surfaces, comparing the DEFAULT and COAREG simulation results (Sect. 3.1, Tab. 1), appears to be limited in terms of relative changes in V_{d,O_3} and the total simulated O_3 deposition budget.

https://doi.org/10.5194/acp-2020-978
Preprint. Discussion started: 29 October 2020

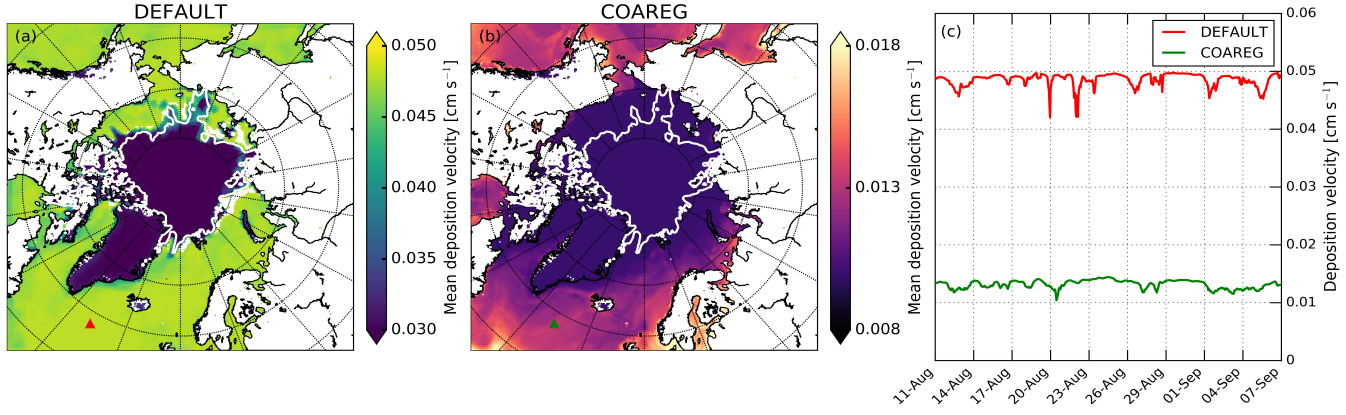

Figure 3. Spatial distribution of the mean simulated O_3 deposition velocity to snow/ice and oceans [cm s^{-1}] for the (a) DEFAULT and (b) COAREG simulations and (c) temporal variation in O_3 deposition velocity [cm s^{-1}] for the DEFAULT (red) and COAREG (green) simulations. The red and green markers in (a) and (b) indicate the location of the time series shown in (c). To give an indication of the sea ice extent, the white contours show the sea ice fraction of 0.5 at the start of the simulation.

Table 1. Mean simulated O_3 deposition velocity (±Standard deviation) [cm s^{-1}] and total simulated deposition budget [Tg O_3 yr^{-1}] for the DEFAULT and COAREG runs to water, snow/ice and land each representing 37%, 15% and 48% of the total surface area respectively.

		Water (37%)	Snow/Ice (15%)	Land (48%)	Total (100%)
DEFAULT	Deposition velocity (±Std.) [cm s^{-1}]	0.048 (±0.003)	0.030 (±0.000)	0.449 (±0.231)	
	Deposition budget [Tg O_3 yr^{-1}]	15.5	4.1	132.9	152.5
COAREG	Deposition velocity (±Std.) [cm s^{-1}]	0.012 (±0.002)	0.010 (±0.000)	0.448 (±0.251)	
	Deposition budget [Tg O_3 yr^{-1}]	4.6	1.7	135.8	142.1

Especially contrasting this with the previously mentioned up to ∼2 orders of magnitude larger V_{d,O_3} to vegetation. However, these relatively small changes do significantly affect the spatial and temporal variation of simulated surface O_3 mixing ratios. Figure 4 shows the spatial distribution in the simulated mean surface O_3 mixing ratios overlain with the observed mean surface O_3 mixing ratios. In the DEFAULT and COAREG runs (Fig. 4a and Fig. 4b respectively) we find similar background O_3 mixing ratios of ∼15-20 ppb over the Russian and Canadian/Alaskan land masses. Over Scandinavia, slightly higher background O_3 mixing ratios of ∼20-25 ppb are simulated due to more anthropogenic emissions of precursors in the EDGAR emission inventory and advection of O_3 and its precursors from outside the domain. We find a limited effect of reduced deposition to water and snow/ice to the simulated mean O_3 mixing ratios over land. In general, the model appears to be able to simulate the mean observed surface O_3 mixing ratios for the Remote and Terrestrial sites (all sites < 70 °N) without clear positive or negative bias. However, we find that the DEFAULT run (Fig. 4a) systematically underestimates the mean observed surface O_3 mixing ratios for the High Arctic sites (all sites > 70 °N) by ∼5-10 ppb likely caused by an overestimated deposition to ocean, snow and ice surfaces. Over the Arctic sea ice and oceans the ABL is typically very shallow and atmospheric turbulence is relatively

https://doi.org/10.5194/acp-2020-978
Preprint. Discussion started: 29 October 2020


Atmospheric Chemistry and Physics Discussions

weak. This suppresses vertical mixing and entrainment of O_3 rich air from the free troposphere. Dry deposition of O_3 to the ocean or snow/ice surfaces appears to be an important removal mechanism that has a large impact on O_3 concentrations in these shallow ABLs both in terms of magnitude but also temporal variability as we will show in Sect. 3.4. In the COAREG run, the background O_3 mixing ratios over oceans and Arctic sea ice have increased up to 50%. Furthermore, the reduced deposition to snow/ice has also clearly affected simulated surface O_3 mixing ratios over Greenland. Most importantly, the negative bias in simulated surface O_3 mixing ratios is reduced in the COAREG run with respect to the DEFAULT run. This is further examined in Sect. 3.3.

The CAMS reanalysis data appears to simulate higher (up to 10 ppb) surface O_3 mixing ratios over land than the two WRF runs. Over sea ice, the magnitude of simulated surface O_3 mixing ratios in CAMS is in between the DEFAULT and COAREG runs. Over Greenland, CAMS simulates mixing ratios of ∼40 ppb, with a sharp gradient towards the coast. This gradient is less pronounced in the WRF simulations. Both CAMS and WRF appear to underestimate the mean observed (∼45 ppb) surface O_3 mixing ratios at Summit. The frequency distributions (Fig. 4d) also show that relatively high (25-45 ppb) simulated surface O_3 mixing ratios are more frequent in COAREG and CAMS compared to the DEFAULT and NUDGED runs.

3.3 Simulated and observed hourly surface ozone

In this section we show how nudging and the application of the revised deposition scheme can especially improve short-term variability in O_3 concentrations reflected in a comparison of the simulated and observed hourly surface O_3 mixing ratios. This is the first time such a oceanic O_3 deposition scheme coupled to a meteorology-chemistry model is evaluated against a large dataset hourly surface O_3 observations. Figure 5 shows a comparison between observed and simulated hourly surface O_3 mixing ratios subdivided in the three site selections: High Arctic, Remote and Terrestrial. For the High Arctic sites (Fig. 5, top row) we again find that the DEFAULT run is underestimating the observed surface O_3 mixing ratios with a mean bias of -7.7 ppb. This is consistent to findings in Fig. 4, where the DEFAULT run appears to underestimate surface O_3 mixing ratios in the High Arctic region. Interestingly, nudging to ERA5 wind, temperature and humidity appears to already reduce some of the bias in the High Arctic by better representing the temporal variability in surface O_3. This is further examined in Sect. 3.4. However, the NUDGED run appears to still underestimate High Arctic surface O_3 with a bias of -3.8 ppb. The COAREG run, having a reduced O_3 deposition sink to oceans and snow/ice appears to better represent the background surface O_3 with a slight positive bias of 0.3 ppb. The MAE in the COAREG run is reduced to 4.7 ppb from 8.5 and 6.4 for the DEFAULT and NUDGED runs respectively. Furthermore, we find that the CAMS reanalysis data also underestimates surface O_3 in the High Arctic with a bias of -5.0 ppb and a MAE of 6.8 ppb. It has to be noted that the performance for all WRF runs and CAMS reanalysis product is varying for each observational site which is further examined in Sect. 3.4.

For the Remote sites (Fig. 5, middle row), having no clear diurnal cycle in surface O_3, we find again an improvement by nudging the WRF model to ERA5 and also by including the mechanistic ocean deposition routine and reduced snow/ice deposition. This improvement appears to be most pronounced for coastal sites like Storhofdi (63.4°N,20.3°W) and Inuvik (68.4°N,133.7°W) having a reduction in the MAE of 57% and 36% respectively (not shown here). Overall, the improvement for the NUDGED and COAREG runs compared to the DEFAULT run in the Remote site selection is not as significant compared to the High

https://doi.org/10.5194/acp-2020-978
Preprint. Discussion started: 29 October 2020

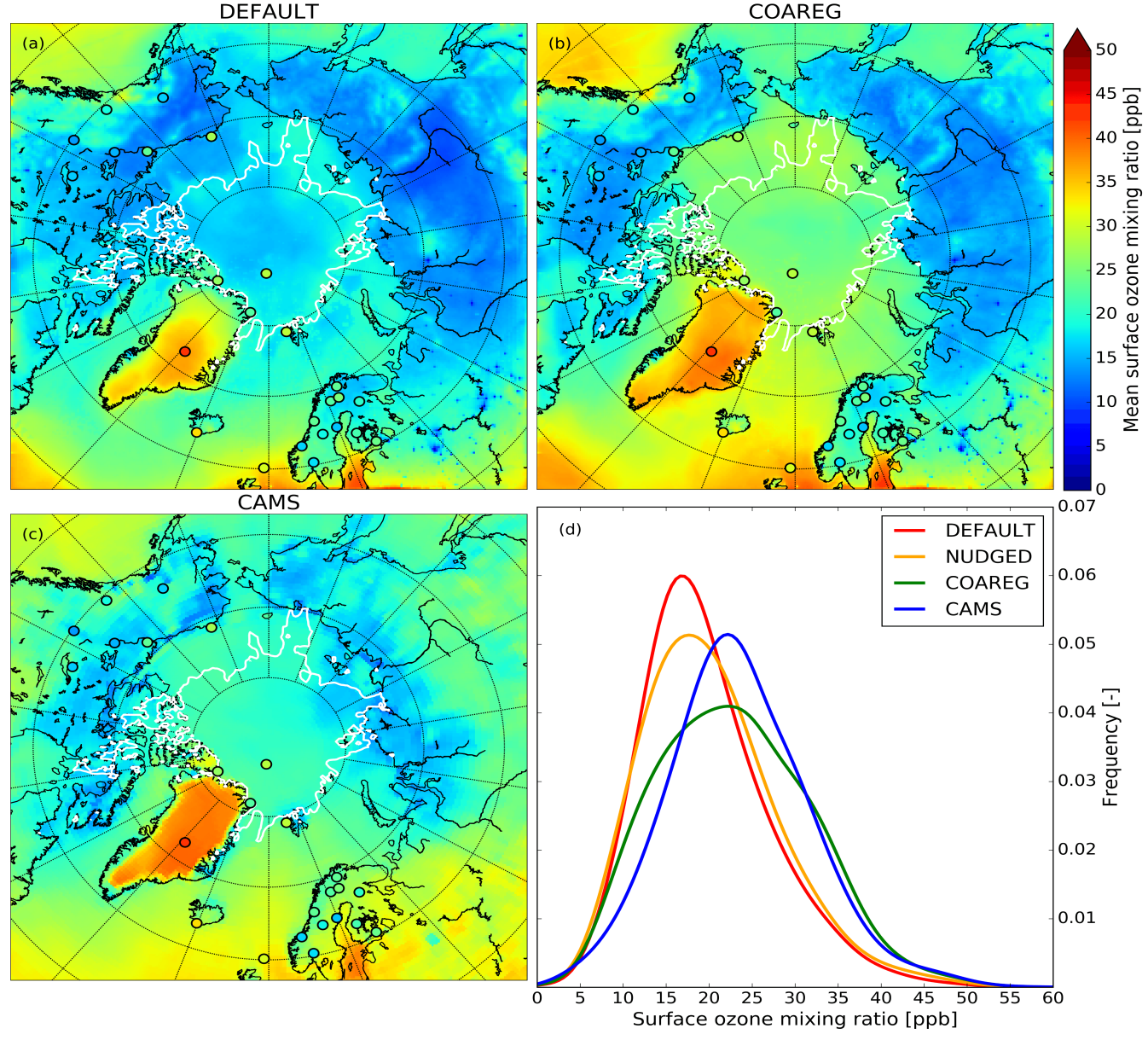

Figure 4. Spatial distribution of the simulated mean surface O_3 mixing ratio [ppb] for the (a) DEFAULT and (b) COAREG runs and (c) CAMS data and (d) frequency distributions of surface O_3 mixing ratios [ppb] over the entire simulation and domain for the DEFAULT (red), NUDGED (yellow), COAREG (green) runs and CAMS data (blue). The filled circles indicate the mean observed ozone mixing ratios [ppb] for the simulated period. To indicate the sea ice extent, the white contours show the sea ice fraction of 0.5 at the start of the simulation.

https://doi.org/10.5194/acp-2020-978
Preprint. Discussion started: 29 October 2020


Atmospheric Chemistry and Physics Discussions

Arctic sites, probably because of the larger role of O_3 deposition to land and vegetation, which remained unchanged in this study. We find that the CAMS data shows the best performance for the Remote sites with no bias and with a MAE of 5.6 ppb. For the Terrestrial sites (Fig. 5, bottom row), having a clear diurnal cycle in surface O_3, all WRF runs slightly overestimate the observed surface O_3 mixing ratios with a mean bias up to 1.0 ppb. By nudging WRF to ERA5 the bias is reduced from 7.0 ppb to 6.0 ppb. Reducing the O_3 deposition to oceans and snow/ice increases the bias, but the MAE remains unchanged. The CAMS reanalysis data appears to perform worst for the Terrestrial sites with a bias of 6.4 ppb and a MAE of 8.0 ppb. This might be explained by the lower spatial and temporal resolution in the dataset at these sites with a relatively strong diurnal cycle in ABL dynamics and O_3 concentrations.

Interestingly, of all the combinations, we find the largest MAE (8.5 ppb) for the High Arctic sites in the DEFAULT run (Fig. 6a) while we find the lowest MAE (4.7 ppb) for the High Arctic sites in the COAREG run (Fig. 6c). This indicates the high sensitivity of the adjusted ocean, snow and ice surfaces deposition representation to the magnitude and temporal variability in surface O_3 at high latitudes. Because these sites are located far away from the domain boundaries we expect that these model results are to a lesser extent influenced by the boundary conditions compared to the Terrestrial and Remote sites and therefore more sensitive to the deposition scheme in WRF.

3.4 Temporal variability of surface ozone in the High Arctic

In Sect. 3.3 we have shown how nudging the WRF model to ERA5 synoptic conditions and revising the O_3 deposition scheme to oceans and snow/ice can improve the model's capability to represent the observed hourly surface O_3 mixing ratios, especially for the High Arctic sites. In this section we show how the three WRF runs and CAMS represent the temporal variation in High Arctic surface O_3 observations, focusing on a selection of the 25 measurement sites. Figure 6 shows the observed and simulated surface O_3 time series for the 6 High Arctic (>70°N) sites: ASCOS, Summit, Villum, Zeppelin, Barrow and Alert. Furthermore, Tab. 2 shows the model skill indicators for the High Arctic sites.

The observations at ASCOS (Fig. 6a) show a sudden increase of surface O_3 mixing ratios from 20 to over 30 ppb around the 17th of August due to advection of relatively ozone rich air during a synoptically active period (Tjernstrom et al., 2012). Only the COAREG run appears to be able to simulate a similar increase in surface O_3 while NUDGED and CAMS show a minor increase and the DEFAULT run shows no increase in simulated surface O_3 at all. From the 17th of August onwards, the observations show mixing ratios between 25 and 35 ppb. The WRF simulations indicate advection of air over ocean and ice surfaces during this time period (not shown here). In the COAREG simulation, with less deposition to these surfaces, surface O_3 mixing ratios are less depleted. Only the COAREG run is able to represent these observed mixing ratios with a bias of -2.0 ppb whereas the other models simulate lower mixing ratios. At Summit (Fig. 6b), we find a large temporal variability in observed surface O_3 between 30 and 55 ppb. From the 11th of August onwards we find a decreasing trend in observed surface O_3 down to 30 ppb before increasing to 40 ppb around the 17th of August. We find that the DEFAULT run is unable to capture this specific event whereas the NUDGED and COAREG runs already appear to capture this event much better in terms of temporal variability even though the model is still biased at the observed minimum of 30 ppb. Furthermore, we find that the CAMS reanalysis data represents this specific period very well, also in terms of magnitude. Over the entire simulated period,

https://doi.org/10.5194/acp-2020-978
Preprint. Discussion started: 29 October 2020

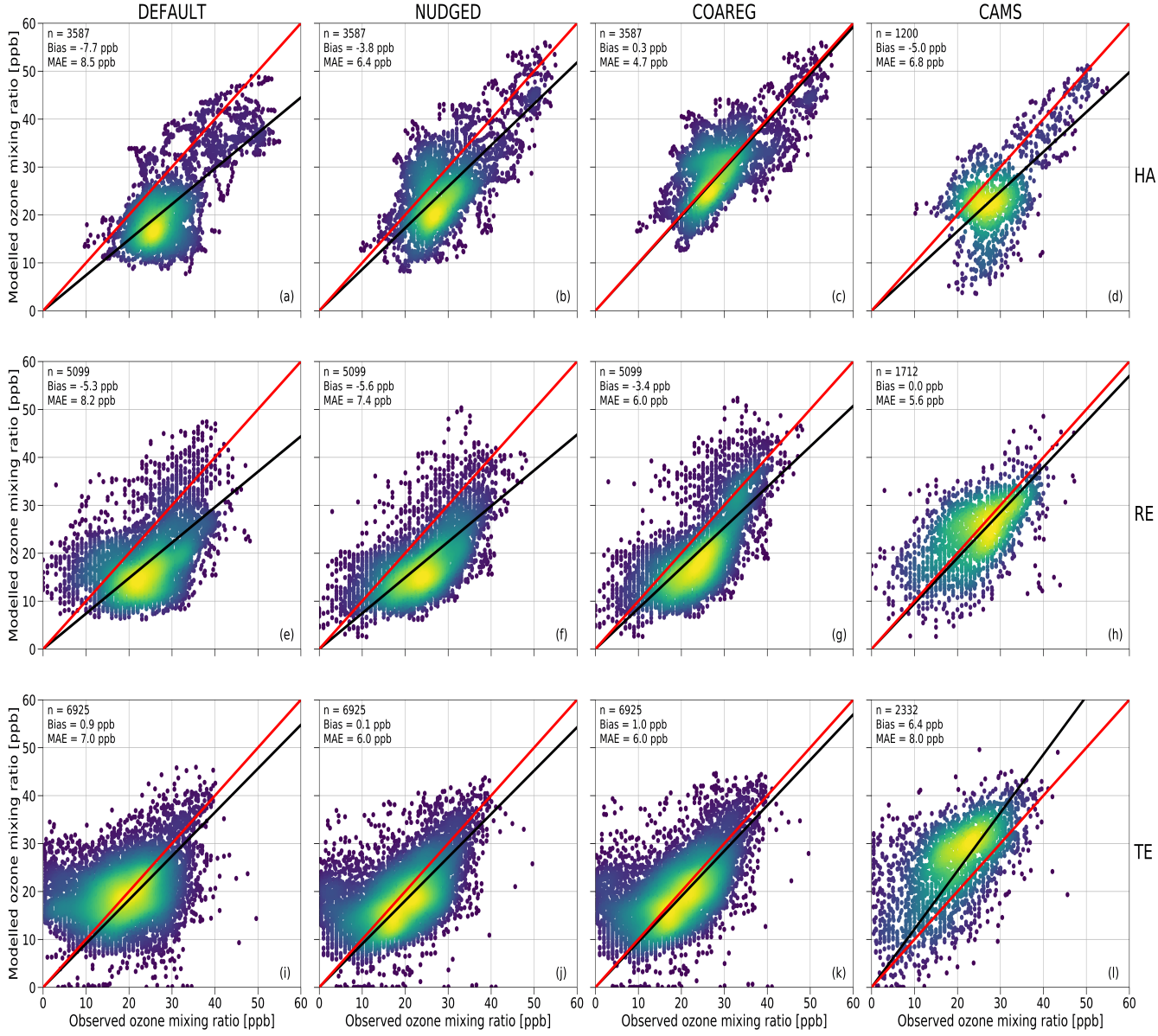

Figure 5. Comparison of the hourly observed and simulated ozone mixing ratios [ppb] for the DEFAULT (a,e,i), NUDGED (b,f,j), COAREG (c,g,k) runs and CAMS data (d,h,l) for the High Arctic (HA) (a-d), Remote (RE) (e-h) and Terrestrial (TE) (i-l) sites. The red line indicates the 1:1 line and the black line indicates the Ordinary Least Squares regression line through the origin. The number of data points (n), Bias [ppb] and Mean Absolute Error (MAE) [ppb] are shown in the top left corner. The colors represent the multivariate kernel density estimation with yellow colors having a higher density.

https://doi.org/10.5194/acp-2020-978
Preprint. Discussion started: 29 October 2020


Atmospheric Chemistry and Physics Discussions

CAMS performs best at Summit with a MAE of 3.9 ppb followed by COAREG with a MAE of 6.1 ppb. Interestingly, Villum (Fig. 6c) is the only site for which the DEFAULT run performs best in terms of bias and MAE. This run slightly underestimates the observed mixing ratios with a bias of -2.4 ppb. The NUDGED and COAREG runs as well as the CAMS reanalysis data all overestimate the observed mixing ratios, especially later into the simulation.

Zeppelin (Fig. 6d) and Barrow (Fig. 6e) show similar behaviour in terms of observation-model comparison. For both locations, both the DEFAULT run as well as the CAMS reanalysis data systematically underestimate observed ozone mixing ratios with biases larger than 10 ppb. In the NUDGED run, some of the temporal variability is already better represented by WRF and reduces the bias to -6.9 and -4.6 ppb for Zeppelin and Barrow, respectively. In the COAREG run the bias is reduced to -1.0 and -0.2 ppb for Zeppelin and Barrow respectively. From the 23th of August until the end of the simulation, we find a good example of the importance of a realistic representation of synoptic conditions by nudging and the role of ocean and snow/ice deposition. In this period, the DEFAULT run and CAMS reanalysis data systematically underestimate the observed surface O_3 mixing ratios. Moreover, the COAREG run is representing the observed surface O_3 mixing ratios very well, both in terms of magnitude as well as temporal variability. At Alert (Fig. 6f), the DEFAULT run again underestimates the observed surface O_3 mixing ratios even though the bias of -6.4 ppb is not as large as for some of the other sites. This bias, as well as the MAE, is again decreased for the NUDGED and COAREG runs. At Alert, we find that CAMS has the lowest MAE of 3.0 ppb, but has a slight negative bias of -1.9 ppb.

The model performance in terms of temporal variability in surface O_3 observations is diagnosed by using the Pearson-R correlation coefficient. Nudging the WRF model to ERA5 meteorological data already improved the representation of the temporal variability especially for sites like Barrow and Summit where the synoptic conditions were likely not represented well. This causes an offset in timing of the advection of different air masses but here also vertical mixing and entrainment of O_3 rich air could play a role. The model performance also improved for all six sites in the COAREG run with respect to the NUDGED run. The COAREG run includes temporal variability in O_3 deposition due to variability in waterside turbulent transport which can explain additional improvements in representing the temporal variability of surface O_3. The COAREG simulation performs best for 5 out of the 6 observational sites in terms of Pearson-R correlation coefficient and is only outperformed by CAMS at Summit.

Overall, we find that nudging reduces the bias and MAE for all High Arctic sites except Summit and Villum by better representing the synoptic conditions and therefore the temporal variability in observed surface O_3. Coupling the WRF model to the mechanistic COAREG ocean-atmosphere exchange representation further decreases the bias and MAE for all High Arctic sites except for Villum by better representing the magnitude of, but also temporal variability in observed surface O_3. The CAMS reanalysis data is performing well for some locations (e.g. Summit, Alert) while for Zeppelin and Barrow the discrepancy is among the largest we found in the observation-model comparison.

https://doi.org/10.5194/acp-2020-978
Preprint. Discussion started: 29 October 2020

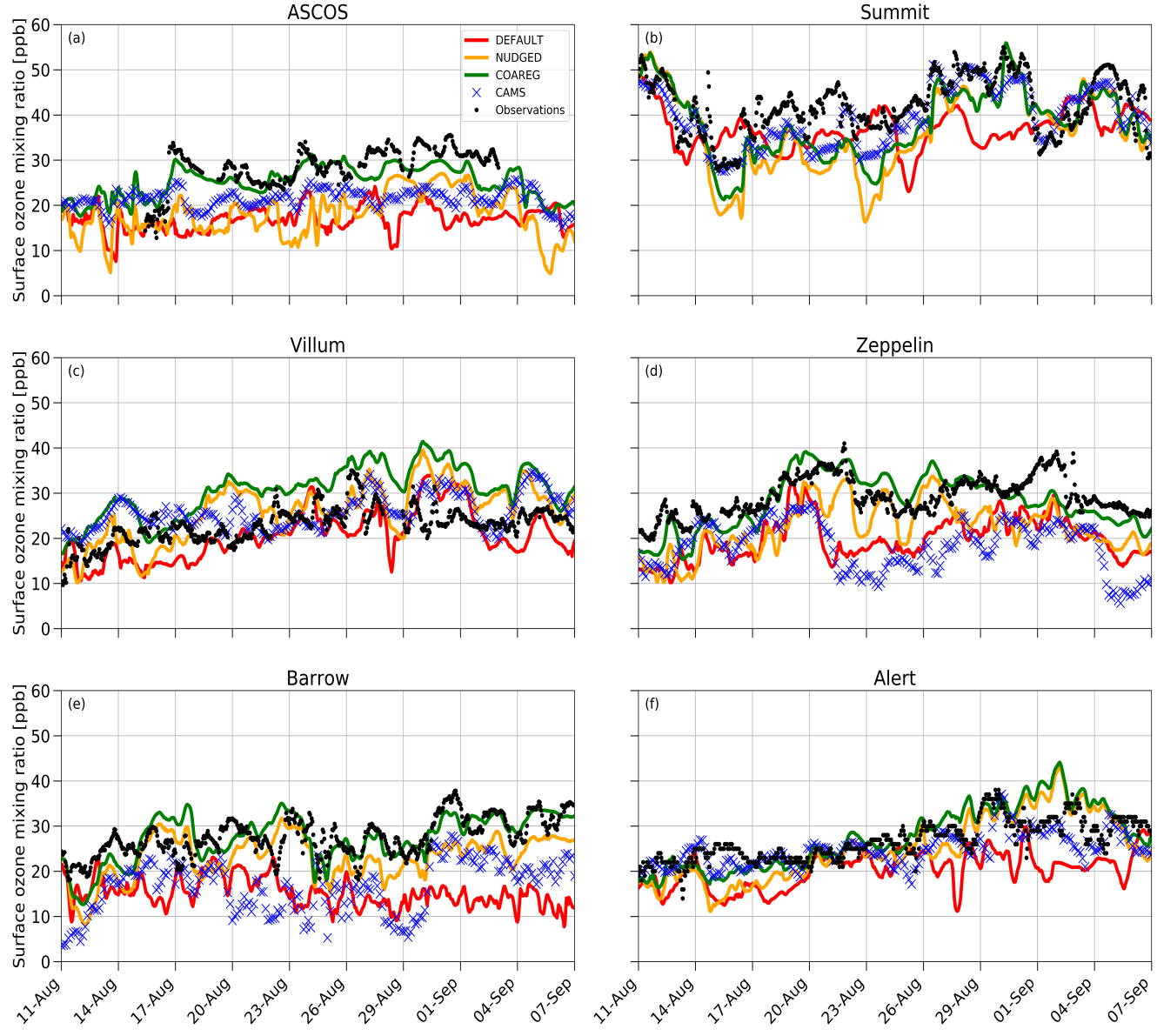

Figure 6. Temporal evolution of hourly surface O_3 mixing ratios [ppb] for the DEFAULT (red), NUDGED (yellow), COAREG (green) runs, CAMS data (blue crosses) and observations (black dots) at ASCOS (∼87.4°N,∼6.0°W), Summit (72.6°N,38.5°W), Villum (81.6°N,16.7°W), Zeppelin (78.9°N,11.9°E), Barrow (71.3°N,156.6°W) and Alert (82.5°N,62.3°W).

https://doi.org/10.5194/acp-2020-978
Preprint. Discussion started: 29 October 2020

Atmospheric Chemistry and Physics Discussions

Table 2. Bias [ppb], MAE [ppb] and Pearson-R correlation coefficient (R) [-] for the DEFAULT, NUDGED, COAREG runs and CAMS re-analysis data at the ASCOS, Summit, Villum, Zeppelin, Barrow and Alert observational sites. The lowest model error and highest correlation have been made bold for every site.

	ASCOS			Summit			Villum			Zeppelin			Barrow			Alert		
	Bias	MAE	R	Bias	MAE	R	Bias	MAE	R	Bias	MAE	R	Bias	MAE	R	Bias	MAE	R
DEFAULT	-11.5	11.5	0.24	-5.3	7.4	0.17	**-2.4**	**4.5**	0.5	-9.5	9.5	0.61	-12.4	12.4	-0.18	-6.4	6.6	0.43
NUDGED	-9.4	9.4	0.46	-5.5	7.5	0.62	3.1	5.4	0.46	-6.9	7.4	0.62	-4.6	5.5	0.49	-1.6	4.4	0.68
COAREG	**-2.0**	**3.1**	**0.67**	-4.0	6.1	0.67	7.5	7.8	**0.6**	**-1.0**	**3.6**	**0.69**	**-0.2**	**3.4**	**0.6**	**0.8**	3.6	**0.74**
CAMS	-6.8	7.5	0.07	**-2.6**	**3.9**	**0.78**	3.0	**4.5**	0.38	-11.1	11.1	0.4	-11.0	11.1	0.56	-1.9	**3.0**	0.65

4 Discussion

In this study, we demonstrate the role of a mechanistic representation of ocean-atmosphere exchange to simulate the magnitude and temporal variability of hourly surface O_3 in the Arctic region. We show that the model sensitivity of the surface O_3 concentrations to the representation of O_3 to ocean, ice and snow surfaces is high, even though the total deposition budget is an order of magnitude smaller than the deposition to land and vegetation. Using a mechanistic representation of O_3 deposition to oceans and reducing the O_3 deposition to snow and ice greatly reduced the negative bias in surface O_3, especially in the high Arctic. Furthermore, the short-term temporal variability in surface O_3 was also better represented by the mechanistic representation of oceanic O_3 deposition by also accounting for temporal variations in the driving processes of O_3 deposition such as waterside turbulent transport.

Our main objective was to address the role of a mechanistic oceanic O_3 deposition representation, including spatial and temporal variability, on the magnitude and temporal variability of surface O_3 concentrations. We show that Arctic surface O_3 concentrations are very sensitive to the representation of O_3 deposition. We did not address include in the presented analysis how the nudging and representation of Arctic O_3 deposition further affects the contribution to the Arctic O_3 budget e.g. by changes in photochemistry and stratosphere-troposphere exchange and advection. For such a budget analysis it would be best to perform at least one year of simulation to also address the seasonal cycles in deposition, photochemistry and long range transport which is computationally too expensive in WRF. Regarding oceanic O_3 deposition this would also include long-term changes in sea ice cover and oceanic biogeochemistry.

The major constraint in this model setup is the lack of oceanic O_3 deposition measurements over the Arctic ocean. The COAREG exchange routine has been built and validated using eddy-covariance measurements over mostly (sub-)tropical waters (Bariteau et al., 2010; Helmig et al., 2012). The COAREG routine has been further developed and used to study the effects of wind speed and sea state on ocean atmosphere gas transfer (Blomquist et al., 2017; Bell et al., 2017; Porter et al., 2020). We do expect that these main drivers, being waterside turbulent transfer and chemical enhancement with dissolved iodide, hold for oceans at high latitudes. Using indirect information to evaluate oceanic O_3 deposition through comparison of surface O_3 observations instead of direct oceanic O_3 flux measurements we show that the addition of this mechanistic representation

https://doi.org/10.5194/acp-2020-978
Preprint. Discussion started: 29 October 2020


Atmospheric Chemistry and Physics Discussions

of O_3 deposition results in a better representation of both the magnitude and temporal variability in surface O_3 observations. However, the exact magnitude and variability in Arctic oceanic O_3 deposition could not be evaluated using flux measurements. Furthermore, we have reduced the deposition to snow and ice based on a study by Helmig et al. (2007a). The results of that study also further motivated follow-up observational and modelling studies aiming at the development of, similar to COAREG for oceanic O_3 deposition, more mechanistic representations of O_3 deposition to snow/ice covered surfaces. For example, efforts have been made to simulate O_3 dynamics in and above the snowpack using a 1D model setup to evaluate observations of O_3 and NO_x concentrations measured above and inside the Summit snowpack (Van Dam et al., 2015). This 1D modelling study showed the main role of aqueous-phase oxidation of O_3 with formic acid in the snowpack (Murray et al., 2015). Comparable 1D modelling studies focused on assessing the role of catalytic ozone loss via bromine radical chemistry in the snowpack interstitial air (Thomas et al., 2011; Toyota et al., 2014). However, these studies mainly arrived at conclusions regarding the role of some of this snowpack chemistry in explaining, partly observed, O_3 concentrations and not so much on snow-atmosphere O_3 fluxes and derived deposition rates that would corroborate the inferred very small O_3 deposition rates by Helmig et al. (2007a). An eddy-covariance system has been set up as part of the MOSAiC campaign and will provide year-round O_3 deposition fluxes to several land surface types such as open ocean and sea ice with fluctuating snow cover. These measurements will further enhance our understanding of O_3 deposition in shallow ABLs at high latitudes and the further role in regional atmospheric chemistry.

In this study we used the COAREG transfer algorithm version 3.6 which is extended with a two-layer scheme for surface resistance compared to the previous versions (Fairall et al., 2007, 2011) and similar to the work by Luhar et al. (2018). Oceanic iodide (I^-_{aq}) is generally deemed to be the most significant reactant for O_3 in ocean water (Chang et al., 2004). Similar to Pound et al. (2019) we have used the global I^-_{aq} distribution by Sherwen et al. (2019) on a spatial resolution of $0.125° \times 0.125°$. This distribution replaces the previously applied iodide estimations only using SST (Chance et al., 2014; MacDonald et al., 2014). Using the Sherwen et al. (2019) distribution for August/September we found relatively high I^-_{aq} concentrations ranging from 30 to 130 nM whereas the MacDonald et al. (2014) estimation would imply I^-_{aq} concentrations ranging from 5 to 50 nM. This implies that in the WRF setup, using the Sherwen et al. (2019) I^-_{aq} distribution, the cold Arctic ocean is still quite effective in removing O_3 from the surface waters having I^-_{aq} as a reactant. On the global scale, the most recent I^-_{aq} climatology by Sherwen et al. (2019) most accurately represents the observed I^-_{aq} compared to estimations only using SST (Chance et al., 2014; MacDonald et al., 2014). However, Sherwen et al. (2019) noted that the I^-_{aq} estimations at high latitudes (north of $\geq$65 °N) are very poorly constrained by the observational datasets and are therefore also an uncertainty in this study on Arctic O_3. Therefore, new I^-_{aq} measurements at high latitudes, for example those performed during the MOSAiC expedition, will be very useful to better constrain the global I^-_{aq} distributions as well as mechanistic oceanic O_3 deposition representations.

The WRF simulations in this study did not consider the additional role of chlorophyll, Dissolved Organic Matter (DOM) or other species such as DMS on chemical enhancement of O_3 in surface waters. Experimental studies have shown that DMS, chlorophyll, or other reactive organics, can enhance the removal of O_3 at the sea surface (Chang et al., 2004; Clifford et al., 2008; Reeser et al., 2009). The global modelling study by Ganzeveld et al. (2009) included a chlorophyll-O_3 reactivity that increased linearly with chlorophyll concentration as a proxy for the role of DOM in oceanic O_3 deposition. The addition of

https://doi.org/10.5194/acp-2020-978
Preprint. Discussion started: 29 October 2020


Atmospheric Chemistry and Physics Discussions

this reaction significantly enhances O_3 deposition to coastal waters such that actually observed O_3 deposition to these coastal waters is well reproduced (Ganzeveld et al., 2009). Other studies on oceanic O_3 deposition such as Luhar et al. (2017); Pound et al. (2019) did not consider the potential role of DOM-O_3 chemistry in oceanic O_3 deposition. The study by Luhar et al. (2018), which did not explicitly consider coastal waters, even suggested that including such a reaction deteriorates the comparison with O_3 flux observations above open oceans. A considerable uncertainty in the DOM-O_3 reaction is the second-order rate coefficient but also the magnitude and variability in oceanic DOM concentrations (Luhar et al., 2018). To test the sensitivity of our model setup to other reactants in the surface water we have performed an additional sensitivity analysis including the chlorophyll-O_3 and DMS-O_3 reactions from Ganzeveld et al. (2009). Regarding chlorophyll we have used the monthly 9×9 km resolution MODIS chlorophyll-α concentrations available at https://modis.gsfc.nasa.gov/data/dataprod/chlor_a.php (last access: 14 Aug 2020). For DMS, we use the monthly climatology from Lana et al. (2011). The sensitivity study with chlorophyll as extra reactant indicated a slight increase (up to 5%) in deposition to coastal waters with chlorophyll concentrations up to 25 mg m^{-3}. However, the resulting effect on surface O_3 concentrations was not significant. Also the reactions with oceanic DMS appear to be weak due to relatively low DMS concentrations in August/September. A potential sensitivity of these reactants on Arctic O_3 deposition could especially be expected in the spring to summer transition following from algal blooms (Stefels et al., 2007; Riedel et al., 2008). However, in springtime the removal of Arctic O_3 near the surface is also largely affected by halogen chemistry (Pratt et al., 2013; Thomas et al., 2013). In this season, the observed surface O_3 mixing ratios can drop to 0 ppb (Halfacre et al., 2014). It this study we have limited our analysis to a period in which halogen chemistry is not important.

We nudged the WRF model to the ECMWF ERA5 reanalysis product to ensure a fair model evaluation with observations due to a better representation of the synoptic conditions. This indicated the important role of the model representation of meteorolog, e.g. advection of polluted air and mixing/entrainment of O_3 in the ABL, in representing the observed surface O_3 concentrations. An improvement in simulated synoptic conditions was also found when initializing and nudging the model with ECMWF ERA-Interim data (Dee et al., 2011). This indicates that both reanalysis products have a better representation of the actual synoptic conditions than the free running WRF model. The model evaluation was set up at a resolution of 30×30 km which is in the order of the ERA5 reanalysis data (0.25°×0.25°) used for initial conditions, boundary conditions and nudging. Nudging, but then to the NCEP FNL reanalysis data, was also applied in a study by Marelle et al. (2017) using WRF for quasi-hemispheric simulations of aerosols and O_3 in the Arctic at a resolution of 100×100 km. In this study we opted for a 30×30 km setup because we expect that the main drivers of tropospheric O_3 (chemical production and destruction, stratosphere-troposphere transport, dry deposition and mixing/advection processes) can be sufficiently resolved at this resolution especially over the relatively homogeneous ocean, ice and snow surfaces. However, we do realize that the use of a 30×30 km might have caused some issues in representing local air flow phenomena such as katabatic winds (Klein et al., 2001) which could explain some of the mismatch at sites like Villum (Nguyen et al., 2016). Another justification for the 30×30 km resolution was to limit computational time and to have a large enough domain to cover the entire region above 60 °N to conduct a large pan-Arctic evaluation while at the same time having all observational sites far enough from the domain boundaries to limit the effect of the imposed meteorological and chemical boundary conditions.

https://doi.org/10.5194/acp-2020-978
Preprint. Discussion started: 29 October 2020


Atmospheric Chemistry and Physics Discussions

We plan to use a similar model setup, but then at a higher resolution or using a 1D-setup, to evaluate the O_3 concentration and flux measurements in and around the Arctic sea ice performed during the year-round MOSAiC expedition. These observations will likely give insight in the role of O_3 deposition to sea ice and the Arctic ocean during different seasons (e.g. wintertime with no photo-chemistry or springtime with active halogen chemistry) and for a wide range of meteorological conditions. Furthermore, this local flux and concentration evaluation can be extended to species such as DMS which is now also included in the COAREG version that is coupled to WRF. However, this lacks a combined seawater and atmospheric concentration and flux dataset to conduct a local validation or a similar pan-Arctic distributed surface network such as presented here for O_3 to perform an indirect regional assessment.

5 Conclusions

The mesoscale meteorology-chemistry model Polar-WRF-Chem was coupled to the Coupled Ocean-Atmosphere Response Experiment Gas transfer algorithm (COAREG) to allow for a mechanistic representation of ocean-atmosphere exchange of trace gases. Regarding the deposition of ozone (O_3) to ocean waters, this mechanistic representation includes the effects of molecular diffusion, solubility, waterside turbulent transfer and chemical enhancement of O_3 uptake through its reactions with dissolved iodide. The new mechanistic representation replaces the constant surface uptake resistance approach often applied in ACTMs. Furthermore, we have increased the O_3 surface uptake resistance to snow and ice. In total, three simulations were performed: 1) default WRF setup (DEFAULT), 2) nudged to ERA5 synoptic conditions (NUDGED) and 3) with adjustments to O_3 surface uptake resistance as described above (COAREG). Furthermore, the CAMS global reanalysis data product has also been included in the comparison to illustrate some limitations in the Arctic. This CAMS product is widely used in air quality assessments and to constrain regional scale modelling experiments. The modelling approach was set up for an end-of-summer period in 2008 and evaluated against hourly surface O_3 at 25 sites for latitudes > 60°N including observations over the Arctic sea ice as part of the ASCOS campaign.

Using the mechanistic representation of ocean-atmosphere exchange, O_3 deposition velocities were simulated in the order of 0.01 cm s^{-1} compared to ∼0.05 cm s^{-1} in the constant surface uptake resistance approach. In the COAREG run, the spatial variability (0.01 to 0.018 cm s^{-1}) in the mean O_3 deposition velocities expressed the sensitivity to chemical enhancement with dissolved iodide. The temporal variability of O_3 deposition velocities (up to ±20% around the mean) is governed by surface wind speeds and expressed differences in waterside turbulent transport. In the constant surface uptake resistance approach, there is no spatial variability in O_3 deposition velocities and the temporal variability is determined by the aerodynamic resistance term that can be significant at low wind speeds. Using the mechanistic representation of ocean-atmosphere exchange reduced the total simulated O_3 deposition budget to water bodies by ∼70% and the increase in surface uptake resistance to snow and ice reduced the deposition budget by ∼60%.

Despite the fact that O_3 deposition to oceans, snow and ice surfaces only constitutes a small term in the total O_3 deposition budget (more than 90% of the deposition is to land), we find a substantial sensitivity to the simulated surface O_3 mixing

https://doi.org/10.5194/acp-2020-978
Preprint. Discussion started: 29 October 2020


Atmospheric Chemistry and Physics Discussions

ratios. In the COAREG run, the simulated mean monthly surface O_3 mixing ratios have increased up to 50% in the typically shallow Arctic ABL above the oceans and (sea-)ice relative to the DEFAULT run. The mechanistic representation of O_3 deposition to oceans, but also nudging to ERA5 synoptic conditions, resulted in a substantial improved representation of surface O_3 observations, especially for the High Arctic sites having latitudes > 70 °N. The DEFAULT run was underestimating the observed surface O_3 mixing ratios with a bias of -7.7 ppb whereas the NUDGED and COAREG runs had a bias of -3.8 ppb and 0.3 ppb, respectively. The evaluation of the WRF runs at individual High Arctic sites showed that using the mechanistic representation of O_3 deposition to oceans and nudging the model to ERA5 better represents the surface O_3 observations in terms of magnitude as well as short-term temporal variability. The evaluation of the CAMS reanalysis product also indicated limitations to represent the observed surface O_3 at the High Arctic in terms of magnitude and temporal variability. Similar to DEFAULT and NUDGED, CAMS underestimated High Arctic observed surface O_3 with a bias of -5.0 ppb indicating that for this product the deposition removal mechanism to oceans and snow/ice might also be overestimated.

This study highlights the role of a mechanistic representation of oceanic O_3 deposition on Arctic surface O_3 concentrations at a high (hourly) temporal resolution. It corroborates the findings of global scale studies and recommends that the representation of O_3 deposition to oceans and snow/ice in global and regional scale ACTMs should be revised. This revision is needed not only to better quantify the O_3 budget at the global scale, but also to better represent the observed magnitude and short-term temporal variability of surface O_3 at the regional scale. On the regional scale, this study also has implications on the fate of the Arctic O_3 budget, Arctic air pollution and climate in a period of declining sea ice and increasing local emissions of precursors. Furthermore, this study also serves as a preparatory study for an extensive evaluation of the upcoming year-round Arctic O_3, and other climate active trace gases, concentration and deposition flux measurements as part of the MOSAiC campaign.

Code availability. The COAREG algorithm is available at ftp://ftp1.esrl.noaa.gov/BLO/Air-Sea/bulkalg/cor3_6/gasflux36/, last access: 10 September 2020. The coupled Polar-WRF-Chem model, model output and post-processing scripts are available upon request.

Author contributions. JGMB, LNG and GJS designed the experiment. JGMB performed the Polar-WRF-Chem simulations, performed the analysis and wrote the manuscript, with contributions from all coauthors.

Competing interests. The authors declare that they have no conflict of interest.

Acknowledgements. J.G.M. Barten is financially supported by the Dutch Research Council (NWO) as part of the Netherlands Polar Programme (NPP) under the project name "Multi-scale model analysis of Arctic surface-boundary layer exchange of climate-active trace gases and aerosol precursors" with grant no. 866.18.004. The authors acknowledge the Polar-WRF-Chem developers and support as well as the COAREG developers and in special Chris Fairall.

https://doi.org/10.5194/acp-2020-978
Preprint. Discussion started: 29 October 2020

Atmospheric Chemistry and Physics Discussions

Appendix A: WRF physical and chemical parameterization schemes.

Table A1. WRF physical and chemical parameterization schemes.

WRF option	Configuration
Physical parameterizations	
Microphysics	WSM5 (Hong et al., 2004)
Long wave radiation	RRTMG (Iacono et al., 2008)
Short wave radiation	RRTMG (Iacono et al., 2008)
Surface layer	Monin-Obukhov (Janjić, 2001)
Land surface	Noah (Chen and Dudhia, 2001)
Boundary layer	MYJ (Janjić, 1994)
Cumulus	Kain-Fritsch (Kain, 2004)
Chemistry	
Gas-phase	CBM-Z (Gery et al., 1989; Zaveri and Peters, 1999)
Photolysis	Fast-J (Wild et al., 2000)
Emissions	
Anthropogenic	EDGAR (Janssens-Maenhout et al., 2017)
Biogenic	MEGAN (Guenther et al., 2012)

https://doi.org/10.5194/acp-2020-978
Preprint. Discussion started: 29 October 2020

Atmospheric Chemistry and Physics Discussions

Appendix B: Surface ozone measurement sites.

Table B1. Surface ozone measurement sites subdivided in the 'High Arctic', 'Remote' and 'Terrestrial' site selections.

Name	Abbreviation	Group	Latitude [°N]	Longitude [°E]
Alert	ALT	High Arctic	82.5	-62.3
ASCOS	ASC	High Arctic	∼ 87.4	∼ -6.0
Barrow	BRW	High Arctic	71.3	-156.6
Zeppelin	NYA	High Arctic	78.9	11.9
Summit	SUM	High Arctic	72.6	-38.5
Villum	VIL	High Arctic	81.6	-16.7
Denali NP	DEN	Remote	63.7	-149.0
Esrange	ESR	Remote	67.9	21.1
Karasjok	KAS	Remote	69.5	25.2
Inuvik	INU	Remote	68.4	-133.7
Lerwick	SIS	Remote	60.1	-1.2
Pallas	PAL	Remote	68.0	21.1
Storhofdi	ICE	Remote	63.4	-20.3
Yellowknife	YEL	Remote	62.5	-114.4
Ahtari	AHT	Terrestrial	62.6	24.2
Bredkalen	BRE	Terrestrial	63.9	15.3
Fort Liard	FOR	Terrestrial	60.2	-123.5
Hurdal	HUR	Terrestrial	60.4	11.1
Karvatn	KRV	Terrestrial	62.8	8.9
Norman Wells	NOR	Terrestrial	65.3	-123.8
Oulanka	OUX	Terrestrial	66.3	29.4
Tustervatn	TUV	Terrestrial	65.8	13.9
Vindeln	VDI	Terrestrial	64.3	19.8
Virolahti	VIR	Terrestrial	60.5	27.7
Whitehorse	WHI	Terrestrial	60.7	-135.0

https://doi.org/10.5194/acp-2020-978
Preprint. Discussion started: 29 October 2020

Atmospheric Chemistry and Physics Discussions

References

Ainsworth, E. A., Yendrek, C. R., Sitch, S., Collins, W. J., and Emberson, L. D.: The effects of tropospheric ozone on net primary productivity and implications for climate change, Annual review of plant biology, 63, 637–661, 2012.

Arnold, S. R., Law, K. S., Brock, C. A., Thomas, J. L., Starkweather, S. M., von Salzen, K., Stohl, A., Sharma, S., Lund, M. T., Flanner, M. G., et al.: Arctic air pollution: Challenges and opportunities for the next decade, Elementa: Science of the Anthropocene, 2016.

Bariteau, L., Helmig, D., Fairall, C., Hare, J., Hueber, J., and Lang, E.: Determination of oceanic ozone deposition by ship-borne eddy covariance flux measurements, Atmospheric Measurement Techniques, 3, 441–455, 2010.

Bell, T. G., Landwehr, S., Miller, S. D., De Bruyn, W. J., Callaghan, A. H., Scanlon, B., Ward, B., Yang, M., and Saltzman, E. S.: Estimation of bubble-mediated air-sea gas exchange from concurrent DMS and CO2 transfer velocities at intermediate-high wind speeds, Atmospheric Chemistry and Physics, 17, 9019–9033, 2017.

Blomquist, B., Brumer, S., Fairall, C., Huebert, B., Zappa, C., Brooks, I., Yang, M., Bariteau, L., Prytherch, J., Hare, J., et al.: Wind speed and sea state dependencies of air-sea gas transfer: Results from the high wind speed gas exchange study (HiWinGS), Journal of Geophysical Research: Oceans, 122, 8034–8062, 2017.

Bromwich, D. H., Otieno, F. O., Hines, K. M., Manning, K. W., and Shilo, E.: Comprehensive evaluation of polar weather research and forecasting model performance in the Antarctic, Journal of Geophysical Research: Atmospheres, 118, 274–292, 2013.

Chance, R., Baker, A. R., Carpenter, L., and Jickells, T. D.: The distribution of iodide at the sea surface, Environmental Science: Processes & Impacts, 16, 1841–1859, 2014.

Chang, W., Heikes, B. G., and Lee, M.: Ozone deposition to the sea surface: chemical enhancement and wind speed dependence, Atmospheric Environment, 38, 1053–1059, 2004.

Chen, F. and Dudhia, J.: Coupling an advanced land surface–hydrology model with the Penn State–NCAR MM5 modeling system. Part I: Model implementation and sensitivity, Monthly weather review, 129, 569–585, 2001.

Clifford, D., Donaldson, D., Brigante, M., D'Anna, B., and George, C.: Reactive uptake of ozone by chlorophyll at aqueous surfaces, Environmental science & technology, 42, 1138–1143, 2008.

Cooper, O. R., Parrish, D., Ziemke, J., Cupeiro, M., Galbally, I., Gilge, S., Horowitz, L., Jensen, N., Lamarque, J.-F., Naik, V., et al.: Global distribution and trends of tropospheric ozone: An observation-based review, 2014.

Dee, D. P., Uppala, S. M., Simmons, A., Berrisford, P., Poli, P., Kobayashi, S., Andrae, U., Balmaseda, M., Balsamo, G., Bauer, d. P., et al.: The ERA-Interim reanalysis: Configuration and performance of the data assimilation system, Quarterly Journal of the royal meteorological society, 137, 553–597, 2011.

Fairall, C., Helmig, D., Ganzeveld, L., and Hare, J.: Water-side turbulence enhancement of ozone deposition to the ocean, Atmospheric Chemistry and Physics, 2007, 443–451, 2007.

Fairall, C., Yang, M., Bariteau, L., Edson, J., Helmig, D., McGillis, W., Pezoa, S., Hare, J., Huebert, B., and Blomquist, B.: Implementation of the Coupled Ocean-Atmosphere Response Experiment flux algorithm with CO2, dimethyl sulfide, and O3, Journal of Geophysical Research: Oceans, 116, 2011.

Fairall, C. W., Bradley, E. F., Rogers, D. P., Edson, J. B., and Young, G. S.: Bulk parameterization of air-sea fluxes for tropical ocean-global atmosphere coupled-ocean atmosphere response experiment, Journal of Geophysical Research: Oceans, 101, 3747–3764, 1996.

Ganzeveld, L., Helmig, D., Fairall, C., Hare, J., and Pozzer, A.: Atmosphere-ocean ozone exchange: A global modeling study of biogeochemical, atmospheric, and waterside turbulence dependencies, Global Biogeochemical Cycles, 23, 2009.

https://doi.org/10.5194/acp-2020-978
Preprint. Discussion started: 29 October 2020

Gaudel, A., Cooper, O. R., Chang, K.-L., Bourgeois, I., Ziemke, J. R., Strode, S. A., Oman, L. D., Sellitto, P., Nédélec, P., Blot, R., et al.: Aircraft observations since the 1990s reveal increases of tropospheric ozone at multiple locations across the Northern Hemisphere, Science Advances, 6, eaba8272, 2020.

Gery, M. W., Whitten, G. Z., Killus, J. P., and Dodge, M. C.: A photochemical kinetics mechanism for urban and regional scale computer modeling, Journal of Geophysical Research: Atmospheres, 94, 12 925–12 956, 1989.

Grell, G. A., Peckham, S. E., Schmitz, R., McKeen, S. A., Frost, G., Skamarock, W. C., and Eder, B.: Fully coupled "online" chemistry within the WRF model, Atmospheric Environment, 39, 6957–6975, 2005.

Guenther, A., Jiang, X., Heald, C., Sakulyanontvittaya, T., Duhl, T., Emmons, L., and Wang, X.: The Model of Emissions of Gases and Aerosols from Nature version 2.1 (MEGAN2. 1): an extended and updated framework for modeling biogenic emissions, 2012.

Halfacre, J., Knepp, T., Shepson, P., Thompson, C., Pratt, K., Li, B., Peterson, P., Walsh, S., Simpson, W., Matrai, P., et al.: Temporal and spatial characteristics of ozone depletion events from measurements in the Arctic, Atmospheric Chemistry and Physics, 14, 4875, 2014.

Hardacre, C., Wild, O., and Emberson, L.: An evaluation of ozone dry deposition in global scale chemistry climate models, Atmospheric Chemistry and Physics, 15, 6419–6436, 2015.

Helmig, D., Ganzeveld, L., Butler, T., and Oltmans, S.: The role of ozone atmosphere-snow gas exchange on polar, boundary-layer tropospheric ozone? a review and sensitivity analysis, 2007a.

Helmig, D., Oltmans, S. J., Carlson, D., Lamarque, J.-F., Jones, A., Labuschagne, C., Anlauf, K., and Hayden, K.: A review of surface ozone in the polar regions, Atmospheric Environment, 41, 5138–5161, 2007b.

Helmig, D., Cohen, L. D., Bocquet, F., Oltmans, S., Grachev, A., and Neff, W.: Spring and summertime diurnal surface ozone fluxes over the polar snow at Summit, Greenland, Geophysical research letters, 36, 2009.

Helmig, D., Lang, E., Bariteau, L., Boylan, P., Fairall, C., Ganzeveld, L., Hare, J., Hueber, J., and Pallandt, M.: Atmosphere-ocean ozone fluxes during the TexAQS 2006, STRATUS 2006, GOMECC 2007, GasEx 2008, and AMMA 2008 cruises, Journal of Geophysical Research: Atmospheres, 117, 2012.

Hersbach, H., Bell, B., Berrisford, P., Hirahara, S., Horányi, A., Muñoz-Sabater, J., Nicolas, J., Peubey, C., Radu, R., Schepers, D., et al.: The ERA5 global reanalysis, Quarterly Journal of the Royal Meteorological Society, 2020.

Hines, K. M. and Bromwich, D. H.: Development and testing of Polar Weather Research and Forecasting (WRF) model. Part I: Greenland ice sheet meteorology, Monthly Weather Review, 136, 1971–1989, 2008.

Hong, S.-Y., Dudhia, J., and Chen, S.-H.: A revised approach to ice microphysical processes for the bulk parameterization of clouds and precipitation, Monthly weather review, 132, 103–120, 2004.

Iacono, M. J., Delamere, J. S., Mlawer, E. J., Shephard, M. W., Clough, S. A., and Collins, W. D.: Radiative forcing by long-lived greenhouse gases: Calculations with the AER radiative transfer models, Journal of Geophysical Research: Atmospheres, 113, 2008.

Inness, A., Ades, M., Agustí-Panareda, A., Barré, J., Benedictow, A., Blechschmidt, A.-M., Dominguez, J. J., Engelen, R., Eskes, H., Flemming, J., Huijnen, V., Jones, L., Kipling, Z., Massart, S., Parrington, M., Peuch, V.-H., Razinger, M., Remy, S., Schulz, M., and Suttie, M.: The CAMS reanalysis of atmospheric composition, Atmospheric Chemistry and Physics, 19, 3515–3556, https://doi.org/10.5194/acp-19-3515-2019, https://www.atmos-chem-phys.net/19/3515/2019/, 2019.

Janjić, Z. I.: The step-mountain eta coordinate model: Further developments of the convection, viscous sublayer, and turbulence closure schemes, Monthly weather review, 122, 927–945, 1994.

Janjić, Z. I.: Nonsingular implementation of the Mellor-Yamada level 2.5 scheme in the NCEP Meso model, 2001.

https://doi.org/10.5194/acp-2020-978
Preprint. Discussion started: 29 October 2020

Atmospheric Chemistry and Physics Discussions

Janssens-Maenhout, G., Crippa, M., Guizzardi, D., Muntean, M., Schaaf, E., Dentener, F., Bergamaschi, P., Pagliari, V., Olivier, J., Peters, J., et al.: EDGAR v4.3.2 Global Atlas of the three major Greenhouse Gas Emissions for the period 1970–2012, Earth Syst. Sci. Data Discuss, 2017.

Kain, J. S.: The Kain–Fritsch convective parameterization: an update, Journal of applied meteorology, 43, 170–181, 2004.

Klein, T., Heinemann, G., Bromwich, D. H., Cassano, J. J., and Hines, K. M.: Mesoscale modeling of katabatic winds over Greenland and comparisons with AWS and aircraft data, Meteorology and Atmospheric Physics, 78, 115–132, 2001.

Lana, A., Bell, T., Simó, R., Vallina, S., Ballabrera-Poy, J., Kettle, A., Dachs, J., Bopp, L., Saltzman, E., Stefels, J., et al.: An updated climatology of surface dimethlysulfide concentrations and emission fluxes in the global ocean, Global Biogeochemical Cycles, 25, 2011.

Law, K. S., Roiger, A., Thomas, J. L., Marelle, L., Raut, J.-C., Dalsøren, S., Fuglestvedt, J., Tuccella, P., Weinzierl, B., and Schlager, H.: Local Arctic air pollution: Sources and impacts, Ambio, 46, 453–463, 2017.

Lelieveld, J. and Dentener, F. J.: What controls tropospheric ozone?, Journal of Geophysical Research: Atmospheres, 105, 3531–3551, 2000.

Luhar, A. K., Galbally, I. E., Woodhouse, M. T., and Thatcher, M.: An improved parameterisation of ozone dry deposition to the ocean and its impact in a global climate-chemistry model, Atmospheric Chemistry and Physics, 17, 3749, 2017.

Luhar, A. K., Woodhouse, M. T., and Galbally, I. E.: A revised global ozone dry deposition estimate based on a new two-layer parameterisation for air-sea exchange and the multi-year MACC composition reanalysis., Atmospheric Chemistry & Physics, 18, 2018.

MacDonald, S., Gómez Martín, J., Chance, R., Warriner, S., Saiz-Lopez, A., Carpenter, L., and Plane, J.: A laboratory characterisation of inorganic iodine emissions from the sea surface: dependence on oceanic variables and parameterisation for global modelling, Atmospheric Chemistry and Physics, 14, 5841–5852, 2014.

Mahmood, R., von Salzen, K., Norman, A.-L., Galí, M., and Levasseur, M.: Sensitivity of Arctic sulfate aerosol and clouds to changes in future surface seawater dimethylsulfide concentrations., Atmospheric Chemistry & Physics, 19, 2019.

Marelle, L., Thomas, J. L., Raut, J.-C., Law, K. S., Jalkanen, J.-P., Johansson, L., Roiger, A., Schlager, H., Kim, J., Reiter, A., et al.: Air quality and radiative impacts of Arctic shipping emissions in the summertime in northern Norway: from the local to the regional scale, 2016.

Marelle, L., Raut, J.-C., Law, K. S., Berg, L. K., Fast, J. D., Easter, R. C., Shrivastava, M., and Thomas, J. L.: Improvements to the WRF-Chem 3.5.1 model for quasi-hemispheric simulations of aerosols and ozone in the Arctic, Geoscientific Model Development, 10, 3661–3677, https://doi.org/10.5194/gmd-10-3661-2017, https://gmd.copernicus.org/articles/10/3661/2017/, 2017.

Marelle, L., Raut, J.-C., Law, K. S., and Duclaux, O.: Current and Future Arctic Aerosols and Ozone From Remote Emissions and Emerging Local Sources—Modeled Source Contributions and Radiative Effects, Journal of Geophysical Research: Atmospheres, 123, 12–942, 2018.

Muller, J. B., Dorsey, J. R., Flynn, M., Gallagher, M. W., Percival, C. J., Shallcross, D. E., Archibald, A., Roscoe, H. K., Obbard, R. W., Atkinson, H. M., et al.: Energy and ozone fluxes over sea ice, Atmospheric environment, 47, 218–225, 2012.

Murray, K. A., Kramer, L. J., Doskey, P. V., Ganzeveld, L., Seok, B., Van Dam, B., and Helmig, D.: Dynamics of ozone and nitrogen oxides at Summit, Greenland. II. Simulating snowpack chemistry during a spring high ozone event with a 1-D process-scale model, Atmospheric Environment, 117, 110–123, 2015.

Nguyen, Q. T., Glasius, M., Sørensen, L. L., Jensen, B., Skov, H., Birmili, W., Wiedensohler, A., Kristensson, A., Nøjgaard, J. K., and Massling, A.: Seasonal variation of atmospheric particle number concentrations, new particle formation and atmospheric oxidation capacity at the high Arctic site Villum Research Station, Station Nord, 2016.

Nuvolone, D., Petri, D., and Voller, F.: The effects of ozone on human health, Environmental Science and Pollution Research, 25, 8074–8088, 2018.

https://doi.org/10.5194/acp-2020-978
Preprint. Discussion started: 29 October 2020


Atmospheric Chemistry and Physics Discussions

Oltmans, S., Lefohn, A., Shadwick, D., Harris, J., Scheel, H., Galbally, I., Tarasick, D., Johnson, B., Brunke, E.-G., Claude, H., et al.: Recent tropospheric ozone changes–A pattern dominated by slow or no growth, Atmospheric Environment, 67, 331–351, 2013.

Paatero, J., Vaattovaara, P., Vestenius, M., Meinander, O., Makkonen, U., Kivi, R., Hyvärinen, A., Asmi, E., Tjernström, M., and Leck, C.: Finnish contribution to the arctic summer cloud ocean study (ASCOS) expedition, Arctic Ocean 2008, Geophysica, 45, 119–146, 2009.

Pausata, F., Pozzoli, L., Vignati, E., and Dentener, F.: North Atlantic Oscillation and tropospheric ozone variability in Europe: model analysis and measurements intercomparison., Atmospheric Chemistry & Physics, 12, 2012.

Porter, J., de Bruyn, W., Miller, S., and Saltzman, E.: Air/sea transfer of highly soluble gases over coastal waters, Geophysical Research Letters, 47, no–no, 2020.

Pound, R. J., Sherwen, T., Helmig, D., Carpenter, L. J., and Evans, M. J.: Influences of oceanic ozone deposition on tropospheric photochemistry, Atmospheric Chemistry and Physics Discussions, pp. 1–25, 2019.

Prados Roman, C., Cuevas, C. A., Fernandez, R. P., Kinnison, D. E., Lamarque, J. F., and Saiz-lopez, A.: A negative feedback between anthropogenic ozone pollution and enhanced ocean emissions of iodine, 2015.

Pratt, K. A., Custard, K. D., Shepson, P. B., Douglas, T. A., Pöhler, D., General, S., Zielcke, J., Simpson, W. R., Platt, U., Tanner, D. J., et al.: Photochemical production of molecular bromine in Arctic surface snowpacks, Nature Geoscience, 6, 351–356, 2013.

Reeser, D. I., Jammoul, A., Clifford, D., Brigante, M., D'Anna, B., George, C., and Donaldson, D.: Photoenhanced reaction of ozone with chlorophyll at the seawater surface, The Journal of Physical Chemistry C, 113, 2071–2077, 2009.

Riedel, A., Michel, C., Gosselin, M., and LeBlanc, B.: Winter–spring dynamics in sea-ice carbon cycling in the coastal Arctic Ocean, Journal of Marine Systems, 74, 918–932, 2008.

Schmale, J., Arnold, S., Law, K. S., Thorp, T., Anenberg, S., Simpson, W., Mao, J., and Pratt, K.: Local Arctic air pollution: A neglected but serious problem, Earth's Future, 6, 1385–1412, 2018.

Sherwen, T., Chance, R. J., Tinel, L., Ellis, D., Evans, M. J., and Carpenter, L. J.: A machine learning based global sea-surface iodide distribution, Earth System Science Data Discussions, pp. 1–40, 2019.

Stefels, J., Steinke, M., Turner, S., Malin, G., and Belviso, S.: Environmental constraints on the production and removal of the climatically active gas dimethylsulphide (DMS) and implications for ecosystem modelling, Biogeochemistry, 83, 245–275, 2007.

Thomas, J. L., Stutz, J., Lefer, B., Huey, L. G., Toyota, K., Dibb, J. E., and von Glasow, R.: Modeling chemistry in and above snow at Summit, Greenland – Part 1: Model description and results, Atmospheric Chemistry and Physics, 11, 4899–4914, https://doi.org/10.5194/acp-11-4899-2011, https://acp.copernicus.org/articles/11/4899/2011/, 2011.

Thomas, J. L., Raut, J.-C., Law, K. S., Marelle, L., Ancellet, G., Ravetta, F., Fast, J. D., Pfister, G., Emmons, L. K., Diskin, G. S., Weinheimer, A., Roiger, A., and Schlager, H.: Pollution transport from North America to Greenland during summer 2008, Atmospheric Chemistry and Physics, 13, 3825–3848, https://doi.org/10.5194/acp-13-3825-2013, https://www.atmos-chem-phys.net/13/3825/2013/, 2013.

Thompson, C. R., Shepson, P. B., Liao, J., Huey, L. G., Cantrell, C., Flocke, F., and Orlando, J.: Bromine atom production and chain propagation during springtime Arctic ozone depletion events in Barrow, Alaska, Atmospheric Chemistry and Physics, 17, 3401, 2017.

Tjernstrom, M., Birch, C. E., Brooks, I. M., Shupe, M. D., Persson, P. O. G., Sedlar, J., Mauritsen, T., Leck, C., Paatero, J., Szczodrak, M., et al.: Meteorological conditions in the central Arctic summer during the Arctic Summer Cloud Ocean Study (ASCOS), Atmospheric Chemistry and Physics, 12, 6863–6889, 2012.

Toyota, K., McConnell, J., Staebler, R., and Dastoor, A.: Air–snowpack exchange of bromine, ozone and mercury in the springtime Arctic simulated by the 1-D model PHANTAS–Part 1: In-snow bromine activation and its impact on ozone, Atmos. Chem. Phys, 14, 4101–4133, 2014.

https://doi.org/10.5194/acp-2020-978
Preprint. Discussion started: 29 October 2020

Atmospheric Chemistry and Physics Discussions

Van Dam, B., Helmig, D., Toro, C., Doskey, P., Kramer, L., Murray, K., Ganzeveld, L., and Seok, B.: Dynamics of ozone and nitrogen oxides at Summit, Greenland: I. Multi-year observations in the snowpack, Atmospheric Environment, 123, 268–284, 2015.

Wentz, F. and Meissner, T.: AMSR-E/Aqua Daily L3 Global Ascending/Descending .25x.25 deg Ocean Grids, Version 2., 2004.

675 Wesely, M.: Parameterization of surface resistances to gaseous dry deposition in regional-scale numerical models, Atmospheric Environment (1967), 23, 1293–1304, 1989.

Wild, O., Zhu, X., and Prather, M. J.: Fast-J: Accurate simulation of in-and below-cloud photolysis in tropospheric chemical models, Journal of Atmospheric Chemistry, 37, 245–282, 2000.

Zaveri, R. A. and Peters, L. K.: A new lumped structure photochemical mechanism for large-scale applications, Journal of Geophysical
680 Research: Atmospheres, 104, 30 387–30 415, 1999.

Zeller, K.: Wintertime ozone fluxes and profiles above a subalpine spruce–fir forest, Journal of Applied Meteorology, 39, 92–101, 2000.